Kinematic α Tensors and Dynamo Mechanisms in a von Kármán Swirling Flow

F. Ravelet,[1] B. Dubrulle,[2] F. Daviaud,[2] and P.-A. Ratié[1]

[1]*Arts et Metiers ParisTech, DynFluid, 151 boulevard de l'Hôpital, 75013 Paris, France*
[2]*CEA, IRAMIS, SPEC, CNRS URA 2464, SPHYNX, 91191 Gif-sur-Yvette, France*

(Received 18 January 2012; published 12 July 2012)

We provide experimental and numerical evidence of in-blades vortices in the von Kármán swirling flow. We estimate the associated kinematic α-effect tensor and show that it is compatible with recent models of the von Kármán sodium (VKS) dynamo. We further show that depending on the relative frequency of the two impellers, the dominant dynamo mechanism may switch from α^2 to $\alpha - \Omega$ dynamo. We discuss some implications of these results for VKS experiments.

DOI: 10.1103/PhysRevLett.109.024503 PACS numbers: 47.65.−d, 52.65.Kj, 91.25.Cw

The dynamo effect is the conversion from mechanical energy to magnetic energy. It is at the origin of most magnetic fields in the Universe (the Earth, stars, galaxies, etc.) and therefore deserves special attention. The von Kármán sodium experiment (VKS) is at present time one of the three successful liquid metal dynamo experiments. In this experiment, the mechanical energy is provided by two iron counter-rotating impellers in a cylindrical vessel, and the spontaneous conversion into magnetic energy is obtained as soon as one of the impellers rotates faster than 16 Hz [1–3]. The process of how this conversion occurs is, however, still a matter of debate. Indeed, a quasi axial axisymmetric mean magnetic dynamo field is observed in VKS experiment, while an equatorial dipole is expected if the dynamo process only involves the time averaged axisymmetric mean flow [4]. Several models have recently been suggested to explain this observation, based upon the now classical α effect in mean field theory of dynamo [5,6]: in the presence of a nonaxisymmetric fluctuating velocity field, the mean VKS magnetic field satisfies

$$\partial_t \langle \mathbf{B} \rangle = \nabla \times (\langle \mathbf{u} \rangle \times \langle \mathbf{B} \rangle + \langle \overline{\overline{\alpha}} \mathbf{B} \rangle - \overline{\overline{\beta}} \nabla \times \langle \mathbf{B} \rangle), \quad (1)$$

where u_i and B_i are the velocity and magnetic field, $\langle\rangle$ denotes time-azimuthal average and $\overline{\overline{\alpha}}$ and $\overline{\overline{\beta}}$ are second-order tensors depending on $\langle u \rangle$ and $u' = u - \langle u \rangle$. Specifically, it was suggested that vortical coherent structures in between the impeller blades such as pictured in Fig. 1(c) generate highly-correlated nonaxisymmetric velocity-vorticity fluctuations that would result in a non-negligible $\overline{\overline{\alpha}}$ tensor able to produce an axial dipole [7,8]. Kinematic simulations using a numerical model of such vortices indeed reproduce the growth of an axisymmetric axial field as observed in VKS experiments [9]. Numerical simulations [8,10] using *ad hoc* $\overline{\overline{\alpha}}$ tensors in the induction equation and different boundary conditions satisfactorily reproduce the large scale structure of the dynamo magnetic field, provided the nondimensional α parameter is of the order of 2 (ferromagnetic boundary conditions, [8]) or 0.02 if variations of the permeability due to soft iron are taken into account [10]. However, no measurements of the velocity structure in between the blades has been available so far, preventing check of the plausibility of these estimates, and, thus, the soundness of these α models. In the present Letter, we first provide some experimental evidence of these in-blades vortical structures and give more quantitative information on their averaged properties using Reynolds averaged Navier-Stokes (RANS) computational fluid dynamics (CFD) calculations. We then use these results to compute the resulting kinematical α effect. Some implications of these results for VKS experiments are finally discussed. Depending on the relative frequency of the two impellers, the dominant dynamo mechanism may switch from α^2 to $\alpha - \Omega$ dynamo, resulting in onset of dynamical regimes.

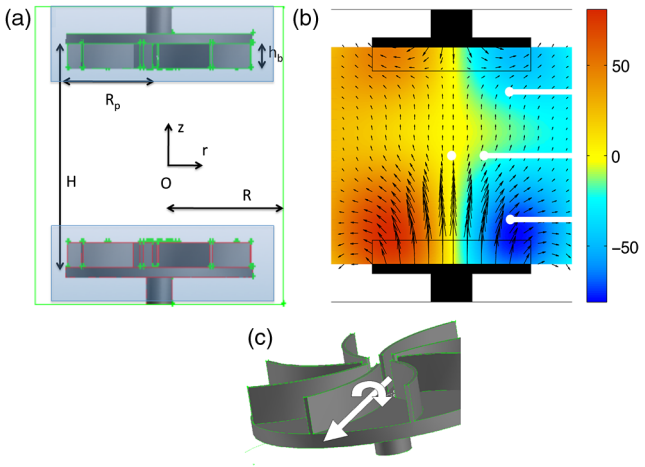

FIG. 1 (color online). (a) Geometry of the experiment. The shaded blue zone denote the rotating fluid volume used in the numerical simulation. (b) Reconstruction of the dynamo magnetic field in a meridional plane in a VKS experiment with rotating bottom disk and stationary upper disk (after [3]). The poloidal (resp. toroidal) component is coded with arrows (resp. color) from blue to red (jet color map). Measuring probes are in white. (c) Putative in-blades vortice creating the α effect.

To observe the vortices potentially responsible for the α effect, we use a von Kármán water experiment which is a $1/2$ scale reproduction of the first successful VKS dynamo experiment described in [1]. Its geometry is summarized in Fig. 1: the fluid contained in a Plexiglas cylinder of radius $R = 100$ mm is stirred by a pair of coaxial impellers that can be rotated independently at rotation frequencies f_1 and f_2 ranging from 1 to 12 Hz. The impellers are flat disks of diameter $2R_p = 150$ mm fitted with either straight blades or radial blades of constant height $h_b = 20$ mm and curvature radius 92.5 mm. The inner faces of the discs are $H = 180$ mm apart. Velocity measurements are performed with a laser doppler velocimetry (LDV) and a stereoscopic particle image velocimetry (PIV) system provided by DANTEC dynamics. In the sequel, we use R and $T = 1/\pi(f_1 + f_2)$ as units of length and time.

In the VKS experiment, dynamo regimes have been observed for a wide variety of rotating frequencies (f_1, f_2) [2]. For simplification, we focus here on the simplest case where the top disk is fixed and the bottom disk is rotating, with the convex face of the blades pushing the fluid forward: $(f_1, f_2) = (1/(\pi T), 0)$. In such a case, dynamo action is observed for $f_1 > 16$ Hz through a nearly axisymmetric dipolar dynamo field, with azimuthal component localized at each impeller [[3,11] and Fig. 1(b)]. Figure 2(a) shows the mean time-averaged nondimensional velocity on a half meridional plane measured by PIV in the experiment. It consists in a fully nonsymmetric flow, with the outside radial part rotating as a block almost at the impeller's velocity. Due to the observing angle, this representation does not allow for velocity measurements inside the blades. Additional measurements using a LDV system and impellers with straight blades allow the measurement of the instantaneous azimuthal velocity component at one point located inside a blade [Fig. 2(b)]. In this measurement, one observes a modulation of the azimuthal velocity, over a period of $1/8f_1$ sec corresponding to one blade crossing. During a period, the azimuthal velocity first drops, and then catches again with the velocity of the blade. This drop results in a smaller averaged velocity (black lower curve) than the impeller velocity (blue upper curve) and is an experimental evidence of the presence of in-blades vortical movements.

To characterize further these motions, we now perform numerical experiments with the CFD finite-volume solver code FLUENT 6.3. The model that has been used is the stationary realizable k-ϵ RANS model [12]. We ran several different mesh configurations before reaching a satisfactory converged solution. It corresponds to a case where the fluid volume is divided into three parts: one central part with a typical element size of 3 mm and two volumes surrounding the impellers 15 mm and 15 mm apart from the blade tips in resp. the axial and radial direction, with conformal interfaces. The mesh is refined to 1 mm close to the blades. The equations are solved in a moving reference frame in one of these volumes to simulate the impeller's rotation. A grid convergence check has been performed and a stable converged solution with one rotating disk was found, with torques at both impellers equal to those measured in the experimental flow within 10 percent. The result is presented in Fig. 2(c) for the azimuthally averaged flow. One observes a one cell circulation close to the experimental one. To quantify this, we present in Fig. 3 a comparison between the numerical and the experimental velocity radial profiles at three locations: $z = \pm 0.53$; $z = 0$. The agreement is within 5% in most of the flow. The CFD solution enables the description of the in-blades velocity. On Fig. 2(c), one observes an intensification of the azimutal velocity at the edge of the rotating impeller, as well as some edge vortices near the top and the bottom edge. In the stationary impeller, the azimuthal velocity is slightly negative, so there is a huge differential rotation at the blades shrouds and tips. The streamlines displayed in Fig. 2(d) enables the clear visualization of in-blades radial trailing vortices, that are located behind the blades. Such vortices can be responsible for a deceleration of the azimuthal velocity observed in Fig. 2(b).

Using the CFD velocity field, one can compute the (nondimensional) azimuthally averaged helicity tensor,

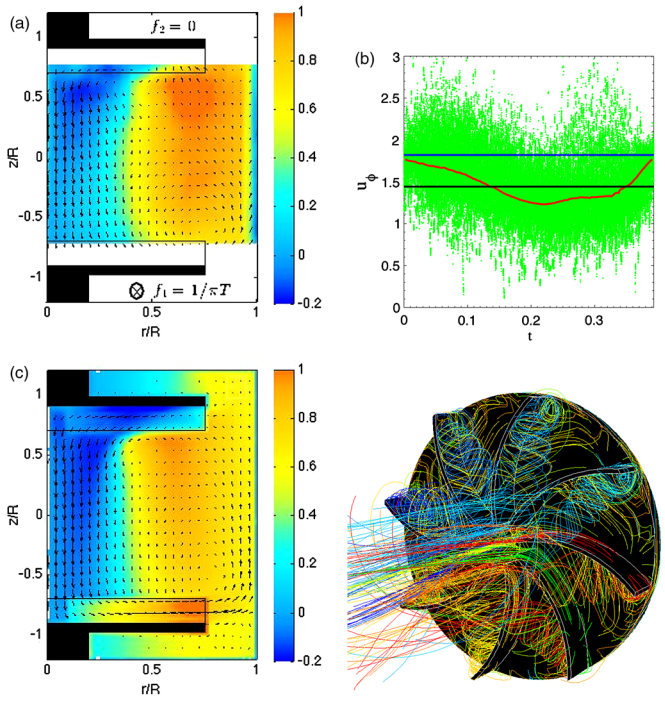

FIG. 2 (color online). (a) Nondimensional experimental mean velocity in a meridional plane. (b) nondimensional azimuthal velocity in the blades synchronized on the blade crossing vs nondimensional time. Green points: LDV measurements; red middle curve: running average; black lower curve: time average; blue upper curve: blade velocity. (c) Nondimensional numerical mean velocity. (d) Radial vortices as observed with streamlines in the CFD simulation.

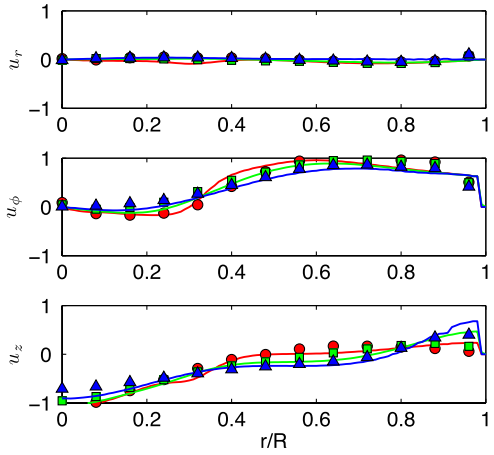

FIG. 3 (color online). Comparison between numerical (line) and experimental (symbols) profiles at $z = -0.53$ (red circles), $z = 0$ (green squares), and $z = 0.53$ (blue triangles). Error bars are of the order of the size of the symbols.

$$h_{ij} = \epsilon_{ikn}\langle u'_k \partial_j u'_n \rangle, \tag{2}$$

where $u' = u - \langle u \rangle$ is the fluctuating velocity field, $h_{ii} = \mathrm{Tr}(h) = -\langle u'_i \omega'_i \rangle$ is minus the helicity of the fluctuations, ω is the vorticity, and the symbol $\langle\rangle$ denotes azimuthal average. The result is displayed in Fig. 4. One sees that the helicity is mainly concentrated in the impellers, with a maximum absolute nondimensional value around 1 (corresponding to 100 ms^{-2} for impeller rotating at 10 Hz). In the rotating impeller, the largest helicity component is $h_{\phi\phi}$ with a value of the order of -0.5. Its value in the stationary impeller is of opposite sign and slightly larger, 1. This difference may be explained by the existence of a very large vertical differential rotation at the stationary impeller, which can generate a large toroidal vorticity. In the rotating impeller, other nonnegligible helicity components are found as $h_{\phi r}$ and h_{rz}. In the stationary impeller, other fairly large helicity components are h_{rr}, $h_{r\phi}$, h_{rz},$h_{z\phi}$, and h_{zr} (of the order of ± 1). We also computed the (nondimensional) azimuthally averaged Reynolds tensor $r_{ij} = \langle u'_i u'_j \rangle$ (not shown). We observed a similar localization of the tensor in the impellers, with a much smaller value, of the order of 5×10^{-2} (corresponding to 0.5 $\mathrm{m}^2\,\mathrm{s}^{-2}$ for impeller rotating at 10 Hz). The exact dynamo properties of such a velocity field would require solving the full kinematic problem, like in [9]. To get an order of magnitude estimates of the dynamo efficiency, we may, however, approximate the fluctuations by a short in time field, since the magnetic Reynolds number in VKS experiment is rather large (between 10 and 70) and the turbulence correlation time is much smaller than the magnetic field diffusive time. In such a case, one can use the computation of [13], equation (29); see also [14] to link the helicity and Reynolds tensor to $\bar{\bar{\alpha}}$ and $\bar{\bar{\beta}}$ as

$$\alpha_{ij} = \tau h_{ij}, \qquad \beta_{ij} = \tau r_{ij}, \tag{3}$$

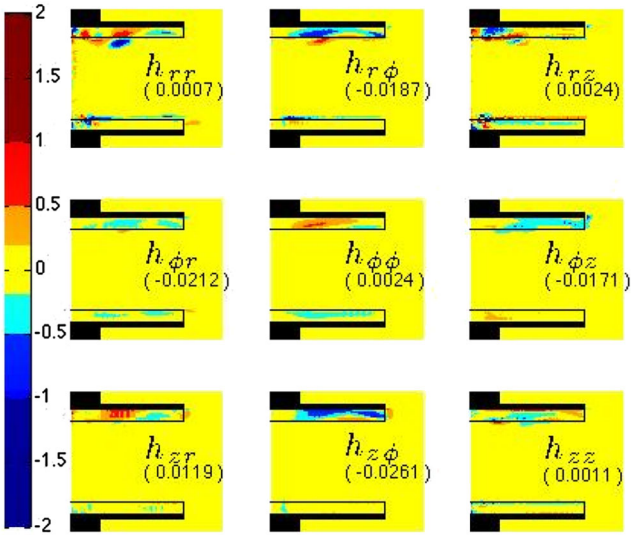

FIG. 4 (color online). Components of the (nondimensional) azimuthally averaged helicity tensor h_{ij} in numerics. The number in parentheses is the volume averaged value.

where τ is the correlation time of the nonaxisymmetric velocity perturbations. The CFD simulation provides a time-independent solution and cannot be used to compute this correlation time. However, we can use the LDV measurements in water (see Fig. 2) to estimate that this time is at most of the order of $1/8f_1$. Therefore, in nondimensional units, $\tau \leq \pi/8$. This estimate leads to maximal nondimensional $\bar{\alpha}$ tensors of the order of ± 0.4 (resp. -0.2) in the stationary (resp. rotating) impeller, and maximal nondimensional $\bar{\bar{\beta}}$ tensors of the order of 2×10^{-2}. Our estimate of $\bar{\alpha}$ using CFD simulations and experiments can be compared with existing models of the VKS dynamo. First, we observe that the largest component of the tensor in the rotating impeller is $\alpha_{\phi\phi}$, as assumed in [8,10]. It is negative, as required for instability [8]. However, its maximal value is an order of magnitude smaller than the value $|\alpha_c| = 2.1$ needed to obtain dynamo action with ferromagnetic boundary conditions at magnetic Reynolds number reached in the VKS experiment [8]. On the other hand, it is one order of magnitudes larger than the value needed to obtain a dynamo action in VKS according to the model with localized permeability distribution [10]. Given the uncertainty in evaluation of the correlation time, we may say that our findings clearly validate the hypotheses of model of [10], but do not rule those of the model of [8]. Dynamo action may be impeded by a large enough turbulent resistivity, parameterized by $\bar{\bar{\beta}}$. This effect has been discarded in the numerical models so far [8,10]. Our estimate shows that this approximation is marginally legitimate in VKS, where the critical magnetic Reynolds number $Rm_c \sim 50$ in our time and length units, resulting in a nondimensional molecular magnetic diffusivity of the order of $1/Rm_c \sim 0.02$, i.e., of the order of the maximal

value for the turbulent magnetic diffusivity, resulting in a 100 percent increase of the total magnetic diffusivity at $Rm = 50$. Our finding is in agreement with a recent estimate of [15] who observed a 50 percent increase of magnetic diffusivity at $Rm = 30$, in a nonstationary turbulent flow of liquid sodium, generated in a closed toroidal channel.

The present computation shows that the in-blade velocity is the VKS impellers is able to generate sufficient α effect to produce a dynamo mechanism, provided adequate boundary conditions [8] or localized permeability distributions [10] are taken into account. The special localization of this α effect found in the present study however calls for further discussion about a qualitative picture of the VKS one disk dynamo. Indeed, using Eq. (1), one can show that the poloidal field (r, z component) is generated from the toroidal field (ϕ component) through the α effect. In contrast, there are two possibilities (possibly concomitant) to generate toroidal field from poloidal field: either through the mean differential rotation $\Omega' = (1/r)d\langle u_\phi \rangle/dz$ (Ω effect) possibly reinforced by the jump of permeability or conductivity at the impellers [16] and (or) through α effect. The first case corresponds to a $\alpha - \Omega$ dynamo, while the second corresponds to an α^2 dynamo. Since the $\bar{\bar{\alpha}}$ tensor varies over a region of size h_b, the crossover in between the two mechanism lies at the critical value $R_p\Omega' \sim \alpha_{rr}/h_b$. This induces a dissymmetry in between the two impellers: at the rotating one, the differential rotation is almost zero $\Omega' \sim 0$ while at the stationary one, the differential rotation occurs over the height of the blades, so that in nondimensional shape $R_p\Omega' \sim R_p/h_b \sim 4$, i.e., is of the order of $\alpha_{rr}R/h_b \sim 4$. Therefore, the dynamo generation is α^2 at the rotating impeller, while it can be a combination of an α^2 and an $\alpha - \Omega$ at the stationary one (an $\alpha^2 - \Omega$) dynamo). Such a dissymmetry may explain generically the field dissymmetry observed in the VKS configuration with one rotating disk, where the field is much more intense near the rotating impeller, than near the stationary impeller cf. Fig. 1.

If the α effect computed in the present case is not strongly modified when the two impellers are rotating, we may draw interesting implications about the VKS dynamo in more general rotating regimes. Indeed, the location of the azimuthal velocity shear layer strongly depends on the relative velocity of the two impellers $\theta = (f_1 - f_2)/(f_1 + f_2)$ [17]: as long as $|\theta| \leq \theta_c$, the azimuthal velocity shear layer is in-between the two impellers, and there is a constant shear at the two impellers, of the order of $\Omega' \approx \pi(f_1 - f_2)/H$. Once $|\theta| \geq \theta_c$, the shear layer is at the slowest impeller, like in the one rotating disk case explored in the present Letter: the differential rotation is almost zero at the fastest impeller, and very strong at the slowest one [18]. This peculiar property however offers possible very different generic dynamo behavior under and above θ_c. For $|\theta| < \theta_c$, the Ω effect is of the order $O(1/H)$, so that it is too weak to supersede the α effect, of the order $1/h_b$ (since $h_b/H \ll 1$). In such case, the dominant dynamo mechanism is α^2 at each impellers. For $|\theta| > \theta_c$, the differential rotation switches to $O(1/h_b)$ at the slowest impeller, and the Ω effect becomes comparable to the α effect. There is therefore the possibility of an $\alpha^2 - \Omega$ mechanism at the slowest impeller, with an α^2 dynamo mechanism at the fastest impeller. This natural switch, induced by the behavior of the shear layer, opens interesting perspectives in terms of possible dynamical regimes in the VKS experiments. Indeed, an homogeneous α^2 dynamo is generically steady, with dynamo threshold $Rm_c = O(k/\alpha)$, while an homogeneous $\alpha - \Omega$ dynamo is generically oscillatory with dynamo threshold $Rm_c = O(k^2\sqrt{(2/\alpha k R_p \Omega')})$, with a rotating frequency bifurcating from a finite value at the dynamo onset $\omega_{osc} = \sqrt{(\alpha k R_p \Omega'/2)}$ [19]. [Meridional circulation and (or) parity properties with respect to the equator of α can steady $\alpha - \Omega$ dynamos.] In our setting, this translates in $Rm_c = O(R/h_b)$ for α^2 dynamos, and $Rm_c = O(R/h_b)/\sqrt{\theta_c/\theta}$ and $\omega_{osc} = O(R/h_b)\sqrt{\theta_c/\theta}$ for the $\alpha - \Omega$ dynamo. Due to inhomogeneities and possible nonlinear coupling in between the two dynamo mechanism at each impeller [3], it is not guaranteed that these generic features will persist. However, we observe that for $\theta < \theta_c$, dynamos observed in VKS are indeed steady, while both steady and dynamical regimes with oscillations appear for $\theta \geq \theta_c$ [20], with oscillation frequency bifurcating from finite value [2]. The scale separation in the VKS experiment, with α and Ω effects occurring in region of size $h_b \ll R$ is in any case a very interesting result, since it validates the main hypotheses underlining the α effect and opens the way to homogenization techniques [21]. It would also be interesting in the VKS experiment to vary the blade's height to see how it affects both the threshold and the oscillation frequencies and check their potential R/h_b scaling.

We thank A. Chiffaudel and F. Bakir for fruitful discussions, P.-P. Cortet for PIV measurements of Fig. 2, and the VKS team for magnetic field measurements used for Fig. 1.

[1] R. Monchaux *et al.*, Phys. Rev. Lett. **98**, 044502 (2007).
[2] R. Monchaux *et al.*, Phys. Fluids **21**, 035108 (2009).
[3] J. Boisson *et al.*, New J. Phys. **14**, 013044 (2012).
[4] F. Ravelet, A. Chiffaudel, F. Daviaud, and J. Léorat, Phys. Fluids **17**, 117104 (2005).
[5] F. Krause and K.-H. Rädler, *Mean-Field Magnetohydrodynamics and Dynamo Theory* (Pergamon, New York, 1980).
[6] H. K. Moffat, *Magnetic Field Generation in Electrically Conducting Fluids* (Cambridge University Press, Cambridge, England, 1978).
[7] F. Petrelis, N. Mordant, and S. Fauve, Geophys. Astrophys. Fluid Dyn. **101**, 289 (2007).

[8] R. Laguerre, C. Nore, A. Ribeiro, J. Léorat, J.-L. Guermond, and F. Plunian, Phys. Rev. Lett. **101**, 104501 (2008); Phys. Rev. Lett. **101**, 219902(E) (2008).
[9] C. J. P. Gissinger, Europhys. Lett. **87**, 39002 (2009).
[10] A. Giesecke, F. Stefani, and G. Gerbeth , Phys. Rev. Lett. **104**, 044503 (2010).
[11] B. Gallet *et al.*, Phys. Rev. Lett. **108**, 144501 (2012).
[12] "FLUENT 6.3 User's Guide," http://hpce.iitm.ac.in/website/Manuals/Fluent_6.3/fluent6.3/help/index.htm.
[13] K.-H. Rädler and M. Rheinhardt, Geophys. Astrophys. Fluid Dyn. **101**, 117 (2007).
[14] A. Brandenburg and K. Subramanian, Astron. Nachr. **328**, 507 (2007).
[15] P. Frick, V. Noskov, S. Denisov, and R. Stepanov, Phys. Rev. Lett. **105**, 184502 (2010).
[16] G. Verhille, N. Plihon, M. Bourgoin, P. Odier, and J.-F. Pinton, New J. Phys. **12**, 033006 (2010).
[17] P.-P. Cortet, P. Diribarne, R. Monchaux, A. Chiffaudel, F. Daviaud, and B. Dubrulle, Phys. Fluids **21**, 025104 (2009).
[18] The value of θ_c is of the order of 0.1 and slightly depends on the blades curvature, the aspect ratio of the experiment, or on the presence of different additional appendices in the flow (ring, baffles, etc.) [17].
[19] P. H. Roberts, Phil. Trans. R. Soc. A **272**, 663 (1972).
[20] M. Berhanu *et al.*, Eur. Phys. J. B **77**, 459 (2010).
[21] B. Dubrulle and U. Frisch, Phys. Rev. A **43**, 5355 (1991).